Hiroshima University Institutional Repository

Size Effect of Hydroxide Nano-Building Blocks and Nonionic Block Co-Polymer Templates on the Formation of Ordered Mesoporous Structures.

Naoki Tarutani[†,‡,§] *, Kiyofumi Katagiri[†], Kei Inumaru[†], and Takamasa Ishigaki[‡,§]

[†] Graduate School of Advanced Science and Engineering, Hiroshima University, 1-4-1, Kagamiyama, Higashi-hiroshima, 739-8527, Japan

[‡] Department of Chemical Science and Technology, Faculty of Bioscience and Applied Chemistry, Hosei University 3-7-2, Kajino-cho, Koganei, 184-8584, Japan

[§] Research Center for Micro-Nano Technology, Hosei University, 3-11-15, Midori-cho, Koganei, 184-0003, Japan

Abstract

The use of pre-crystallized nanoparticles as nano-building blocks (NBBs) is a promising way to obtain mesoporous materials with crystalline walls. In this study, the size effects of both

hydroxide NBBs and nonionic block co-polymers (BCPs) templates on the formation of ordered mesostructures are investigated. The diameter of layered nickel hydroxide NBBs was controlled in sub-2-nm scale by epoxide-mediated alkalinization process. Commercially available nonionic BCPs (gyration radius of 11.9−43.9 Å) were used. Meso-periodic structures formed thorough evaporation-induced self-assembly process. A proper size combination of hydroxide NBBs, smaller than 12.5 Å, and BCPs, larger than 19.9 Å, is shown to be necessary to form ordered meso-structures.

Introduction

Mesoporous materials were discovered in the 1990s[1] and, to date, not only their fundamental science but also their industrial applications have been investigated.[2,3] Although mesoporous materials have been, in general, synthesized using a molecular precursor (for instance metal alkoxides), the use of nanoparticles has been shown to be an alternative route.[4–6] Nanoparticles work as nano-building blocks (NBBs) to construct ordered mesostructures and subsequently mesoporous structures in the process. Mesoporous materials with crystalline matrixes have been easily fabricated by using pre-crystallized NBBs, which is difficult from the preparation through a conventional molecular precursor route because crystallization of the matrix usually collapses the meso-periodic structures.[7] Although NBBs of metals and metal oxides have been used in many reports, owing to their high thermal stability during template removal,[8–10] our group first reported the preparation of well-ordered mesoporous films using metal hydroxide NBBs with varying chemical compositions.[11] The mesoporous materials of layered metal hydroxides are

examples of functional materials that have facilitated a wide variety of application fields, such as batteries and catalysts.[11–13]

The unique properties of mesoporous materials depend on the regular pore size and periodicity on the meso-scale. Regular mesopores enable a control of the reaction space[14,15] and confine low molecular weight species.[16,17] Periodic mesoporous structures are scaffolds with enhanced resonance.[18,19] Therefore, control of the diameter and degree of mesopore ordering are essential factors to determine the functions of these materials. In the case of the NBB route, several characteristics of NBBs, such as diameter, dispersibility, surface charge, diffusion velocity, and interaction with templates, will affect the formation of periodic mesostructures. However, few reports have examined the effects of these factors because precise and independent control of such factors has remained a challenge.

We have recently reported the experimental and simulation study of highly ordered mesoporous structures formation using single-nm-sized layered nickel hydroxide NBBs.[20] Experimental results indicated that inhibition of agglomeration of hydroxide NBBs leads to the formation of highly ordered mesoporous structures. A simulation study suggested that the size ratio between NBBs and template block co-polymers (BCPs) will have a drastic effect on the degree of mesostructure ordering. Although it is known that ordered mesoporous structures were synthesized by using the NBBs less than proper size (< 5 nm in many cases),[4–6,8–10] specific size effect of NBBs and BCPs on the degree of mesopore ordering has not been systematically investigated to our knowledge. Herein, this study focuses on the size difference between hydroxide NBBs and nonionic BCPs to elucidate the influence of the size factor on the formation of ordered mesostructures. Hydroxide NBBs in the size scale of sub-2-nm were prepared as colloids through epoxide-mediated alkalinization. Synthesized hydroxide NBB colloids were

mixed with solutions dissolved of various sized commercially available nonionic BCPs. Ordered mesostructures formed when proper sized hydroxide NBBs and BCPs were employed.

Experimental

Chemicals: Nickel chloride hexahydrate ($NiCl_2 \cdot 6H_2O$, 98.0%), acrylic acid (99.0%), ethanol (99.5%), (±) propylene oxide (>99.0%), and the BCPs listed in Table 2 were used as received. $NiCl_2 \cdot 6H_2O$ was purchased from Wako Pure Chemicals Industries, Ltd (Osaka, Japan). All other reagents were purchased from Sigma-Aldrich Co (St. Louis, state of Missouri, USA). Ultrapure water with a resistivity of 18.2 MΩ·cm was used in all experiments.

Materials synthesis: $NiCl_2 \cdot 6H_2O$ (1.25 mmol) and acrylic acid (2.5 mmol) were dissolved in ethanol (2.5 mL). Propylene oxide (18.75 mmol) was added to the precursor solution. Resultant homogenous solutions were left at room temperature (20−25 °C). After an appropriate time (1−60 min), 2.5 mL of the BCP dissolved ethanoic solutions (BCPs; 5 mmol/L, water; 1.0 mol/L) were added and stirred for 10 s. The obtained solution was immediately transferred to a pre-heated glass petri dish (temperature: 100 °C, size: φ155 mm) and dried in an vacuum oven at 100 °C for 5 min. Powders were obtained by scratching and dried at 60 °C for 3 h. For scanning electron microscopy (SEM) observation, the reacted solutions were dried on a Si substrate instead of a glass petri dish. Part of the samples were heat treated at 200 °C for 2 h in a pre-heated oven and at 250 °C for 6 h with a ramp rate of 1°C/min.

Characterization: In situ data of the conductivity and pH of solutions were collected every 5 s after the reaction started using a water quality meter (D74, Horiba, Japan) with respective glass electrodes (3552-10D and 9618-10D). A transmission electron microscopy (TEM; JEM-2100F, JEOL, Japan) was employed at an operating voltage of 200 kV to observe the mesostructures.

For the TEM observation, the films after heat-treatment at 250 °C were scratched and the obtained fine powders were dispersed in ethanol to form a slightly turbid suspension. A small drop of the resultant suspension was placed on a carbon-coated copper mesh grid and dried at room temperature. A field emission SEM (S-8020, Hitachi, Japan) was used to observe the fine structures of the external surface. A SEM operated with a retarding mode of a low landing voltage of 1 kV (acceleration and deceleration voltage of 2.5 kV and 1.5 kV, respectively) was chosen to observe the external surface structures without structural change induced by an electron beam. X-ray diffraction (XRD) and small angle X-ray scattering (SAXS) patterns of powder samples were taken using SmartLab (Rigaku Corp., Japan) equipped with a one-dimensional detector (D/tex Ultra) using Cu Kα radiation (λ = 0.154 nm) with an accelerating voltage of 30 kV and an applied current of 40 mA. SAXS measurements of solution samples to calculate the size of the BCPs were performed using a SAXSpace system (Anton Paar GmbH, Austria) equipped with a one-dimensional detector (Mythen R 1k) using high-flux sealed-tube X-ray source (CuKα, λ = 0.154 nm) with an accelerating voltage of 40 kV, applied current of 50 mA, and camera length of 317 mm. Obtained slit-collimated SAXS patterns were modified by desmearing procedure. For solution SAXS measurements, BCP dissolved solutions were encapsulated in quartz capillary tubes (φ 1 mm, glass thickness of 10 μm). The temperature was controlled at 25.0 °C during the solution SAXS measurements. Fourier transform infrared (FT-IR) spectra were recorded from 4000−400 cm^{-1} at 4 cm^{-1} resolutions using a FT/IR-4100 spectroscopy (JASCO Corp., Japan) to characterize chemical bonds of synthesized samples. X-ray photoelectron spectrometry (XPS) analyses were carried out with an ESCA-3400 (Shimadzu Corp., Japan) using a monochromatic Mg Kα source (150 W) to evaluate the oxidation state of Ni species. Thermogravimetric-differential thermal analysis (TG-DTA) was carried out at a ramp

rate of 10 °C/min with continuously flow of N_2 (80 mL/min) and O_2 (20 mL/min) gases using a TG-DTA2000S (Mac Science Co., Japan).

Results and discussion

The synthesis and size control of layered nickel hydroxide NBBs followed those reported in a previous work.[20] Ethanolic solutions of dissolved nickel chloride hexahydrate and acrylic acid were used as precursors. Addition of propylene oxide triggered an increase of the solution pH and temperature (Figure 1), which indicated the progress of the exothermic ring-opening reaction of propylene oxide.[21] Nucleophiles in the media determine the reaction rate, *i. e.*, pH increase rate, which affects the shape, size, and chemical composition of precipitating metal hydroxides.[22–24] Decrease of the solution conductivity indicated the formation of NBBs from the ionic precursors. XRD pattern of the NBB showed formation of layered nickel hydroxide intercalated with acrylate (Figure S1). Changes of the solution pH, conductivity, diameter of NBB (d_{NBB}), and relative amount of acrylic acid (f_A) at appropriate reaction times are summarized in Table 1. Subsequently, ethanolic solutions of dissolved BCPs were prepared. The BCPs used in this study are listed in Table 2. SAXS patterns of the BCP dissolved solutions were well fitted to the single structural model using a unified fitting model[25,26] (Figure S2). The gyration radius of the BCPs (r_{BCP}) linearly increased as the number of molecular units of BCPs increased (Figure 2), which agreed with the simulated trend using coarse-grained model.[27] Considering these results and the reported studies,[28,29] BCPs were dispersed as unimers in ethanolic solution. The synthesized hydroxide NBB colloids and BCP dissolved solutions were mixed and subsequently vacuum dried in pre-heated oven at 100 °C for 5 min. Powdery samples were collected by scratching the dried bulks. Here, the sample identifications were denoted by using the BCP name and reaction time in minute-scale, such as F127-1. BCPs could be removed

by heat treatment at 250 °C (Figure S3). Figure 3 and S4 shows SEM and TEM images of the samples after heat-treatment. All the samples showed spherical mesopores, which meant that the BCPs were concentrated beyond the critical micelle concentration and formed spherical micelles during the drying process. The mesopore walls were composed of individual particles (Figure 3c and 3d), which indicated that spherical BCP micelles were successfully surrounded by hydroxide NBBs. The ring pattern of the fast Fourier transformed (FFT) image of heat-treated F127-5 indicated short-range-ordered mesoporous structures (Figure 3a inset). In the case of F108-5, F68-5, P123-5, and L121-5, short-range-ordered mesoporous structures were observed, similar to F127-5. On the other hands, the FFT image of heat-treated L64-5 and L61-5 showed a blurred pattern (Figure 3b inset), which meant that the mesopores were distributed in various periodic length. SEM and TEM observation indicated that ordering of the mesoporous structures depended on the type of BCPs.

Here, we focused on a detailed investigation of the F127 system. XRD patterns and XPS spectra revealed that the heat treatment could lead collapsing layered structure of nickel hydroxides (Figure S5), which may affect the meso-scale ordering. Therefore, dried samples were evaluated for the following discussion. Figure 4 shows the SAXS and XRD patterns of dried powders prepared with F127 BCP. F127-1, F127-3, F127-5, and F127-7 showed peaks at around 0.45 nm^{-1}. This corresponded to a periodicity of 14 nm, which is comparable to the reported value for spin-coated mesoporous thin films.[11,20] It was proposed that hydroxide NBBs and BCP micelles formed ordered mesostructures during drying through an evaporation-induced self-assembly process.[30] However, the peak was weak and broad in the SAXS pattern of F127-10 and there was no obvious peak in the SAXS patterns of F127-15 and F127-60. This indicated that formation of the ordered mesostructures strongly depends on the reaction time, that is, d_{NBB}.

The XRD patterns of the samples other than F127-1 showed the peaks positioned at 2θ = 7.3−8.4 °, which were assigned to a basal plane of the acrylate-intercalated layered nickel hydroxides.[11] Crystallite sizes, D_{NBB}, of basal planes increased with reaction time (Table 1), indicating crystal growth along with pH increasing. Although D_{NBB} and d_{NBB} were comparable after 60 min reaction, D_{NBB} were larger than d_{NBB} after appropriate reaction time (Figure S6), which implies that NBBs rapidly grew during drying at 100 °C. The XRD pattern of F127-1 showed several sharp peaks (crystallite size of 14 nm). These peaks were not detected in the cases of the powders prepared with the BCP-absent precursor solutions, which showed that the peaks could be assigned to layered nickel hydroxide and $NiCl_2 \cdot 2H_2O$ (Figure S7). The crystalline materials may be co-crystals of BCPs and acrylic acid/Ni ionic species considering the large amounts of free acrylic acid and Ni ionic species. In fact, polyethylene oxide (part of BCPs) has been reported to form a co-crystal with small molecules.[31–33] Interaction of BCPs and acrylic acid was supported by IR spectra (Figure S8). F127-15 and F127-60 showed two additional sharp peaks derived from the crystallization of polyethylene oxide chains in the F127 BCP (crystallite size of 14 nm).[34] We have reported a phase separation between polyethylene oxides and layered nickel-based hydroxides during nucleation and crystal growth owing to a relatively weak interaction between polymers and hydroxides.[35] Considering this, a macro-scale phase separation was likely to have taken place between hydroxide NBBs and F127 BCPs in the present study as well. The results of SAXS and XRD measurements are summarized as follows; (1) with a short reaction time, ordered mesostructures were formed along with the formation of BCP-based co-crystals; (2) with a medium reaction time, ordered mesostructures of hydroxide NBBs and F127 BCPs were formed; (3) with a long reaction time, ordered mesostructures were not formed because of the phase separation between hydroxide NBBs and BCPs. The present

results showed a different trend from our previous work on mesoporous materials, in which BCP-based co-crystals or phase-separated BCP crystals were not detected.[11,20,36] This may result from a different drying process; the drying methods of small droplet casting, spin-coating, and spray drying employed in the previous reports take place on a sub-second or second timescale for drying.[37,38] In contrast, the minute timescale is necessary in the case of vacuum drying used in the present study. A longer duration of the drying will allow the formation of co-crystals or phase separation to proceed.

The SAXS and XRD patterns of dried powders prepared using different BCPs are shown in Figure S9 and S10. The trend of the ordered mesostructures formation was the same as that in the discussion written above. With increasing reaction time, the peaks assigned to ordered mesostructures were broadened and disappeared in the cases of the powders prepared using F108, F68, P123, L121, and L64 BCPs. No peak was observed at all in the case of the samples prepared using L61 BCP. BCP-based co-crystals were formed in a short reaction time except for the F108 system. The peaks assigned to the crystalline polyethylene oxide chains of BCP were detected for the sample prepared with a longer reaction time using F108 BCP as well as F127 BCP. The results based on SAXS and XRD patterns are summarized in Figure 5 using r_{BCP}, d_{NBB}, f_A, and the number of polyethylene oxide units in the BCPs (n_{PEO}). Ordered mesostructures were formed in the area with a smaller d_{NBB} and larger r_{BCP}. This clearly indicated that relatively large NBBs, compared with the BCP micelles, inhibited the formation of ordered mesostructures of NBBs and BCP micelles. Here, the critical micelle concentration was assumed to be one of the effective factors for the formation of ordered mesostructures as well; however, no relation was observed in this study considering both the experimental and simulation critical micelle concentration values.[39,40] With regards to the formed crystalline phases, BCP-based co-crystals

were formed from solutions having a large f_A. When the BCPs with a large n_{PEO} were employed, the threshold f_A for the formation of co-crystals increased until finally the co-crystal was not formed. However, in the case of a BCP with a large n_{PEO}, phase separation took place between hydroxide NBBs and BCPs, which resulted in the formation of coarse BCP crystals. Figure 6 represents a schematic illustration of the effects of the sizes of hydroxide NBBs and BCPs on the formation of ordered mesostructures. In the cases of small BCPs, ordered mesostructures were not achieved even when sufficiently small hydroxide NBBs, predicted by simulation study, were employed. This implies that an optimization of other factors, such as interaction between NBBs-NBBs, NBBs-BCPs, and BCPs-BCPs, will be necessary for certain simulations. In addition, particle growth during evaporation of solvent will disturb formation of ordered structures. Ordered mesostructures were formed when BCPs forming medium-sized micelles were employed. With increasing NBB size, the obtained structures changed from ordered structures to disordered structures. Larger micelles enabled the formation of meso-periodic structures even when larger sized NBBs were used. However, phase separation between BCPs and hydroxide NBBs took place if the NBBs employed were too large. This arose from the small interaction between hydroxide NBBs and BCPs compared with that observed between the molecular precursors that are used in conventional methods.

Conclusion

In conclusion, the size effect of both hydroxide NBBs and nonionic BCPs on the formation of ordered mesostructures was evaluated in this study. The size of the hydroxide NBBs was precisely controlled at the sub-2-nm scale through a solution-based synthetic procedure. The

commercially available nonionic BCPs employed were of various sizes that linearly depended on the total unit number. Systematic investigation elucidated that ordered mesostructures were formed when a proper size combination between NBBs and BCPs was employed. In the case of the small micelles, ordered mesostructures were not formed even when sufficiently small NBBs were employed. When large BCPs were employed, phase separation took place between the hydroxide NBBs and BCPs. We believe that the present study will give methodologically critical information to design mesoporous materials composed of nanocrystals.
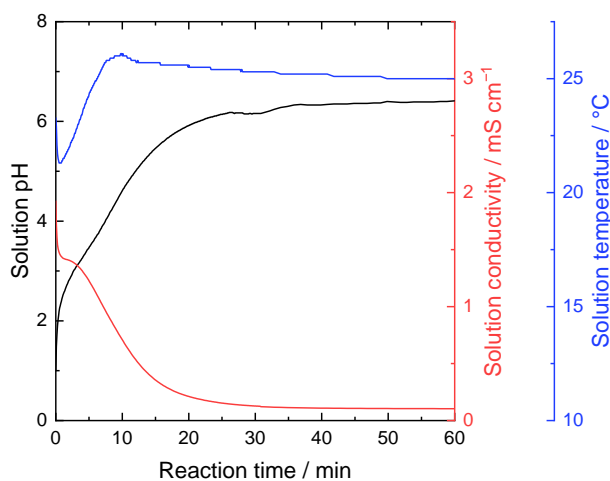

Figure 1. Time dependent change of solution pH (black), conductivity (red), and temperature (blue) after addition of propylene oxide to an ethanolic solution of dissolved $NiCl_2 \cdot 6H_2O$ and acrylic acid.
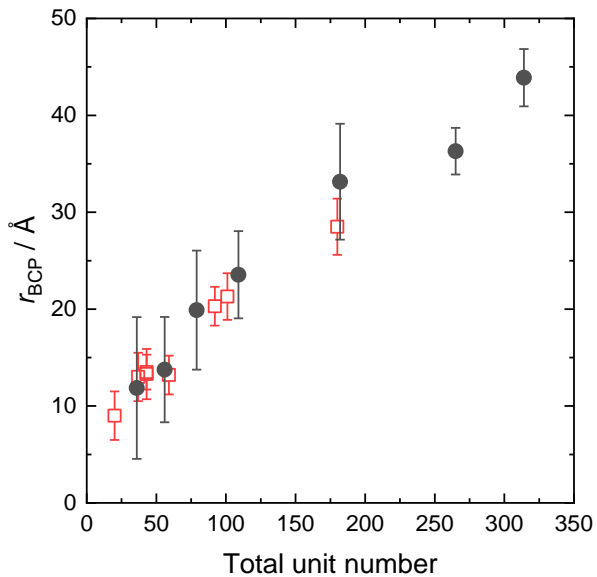
Figure 2. Relationship between total unit number in the BCPs and experimental gyration radius of the BCPs (black close circle). The red open square symbols represent the calculated gyration radius of the BCPs reported elsewhere.[27] Copyright 2014 American Chemical Society.
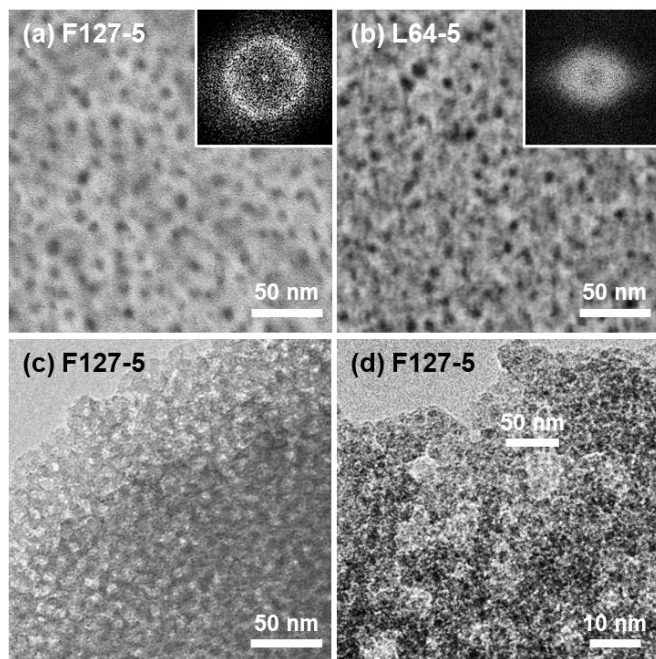

Figure 3. (a) (b) SEM and (c) (d) TEM images of F127-5 and L64-5 after heat treatment at 200 °C for 2 h and 250 °C for 6h. Insets of (a) and (b) are the corresponding FFT images.
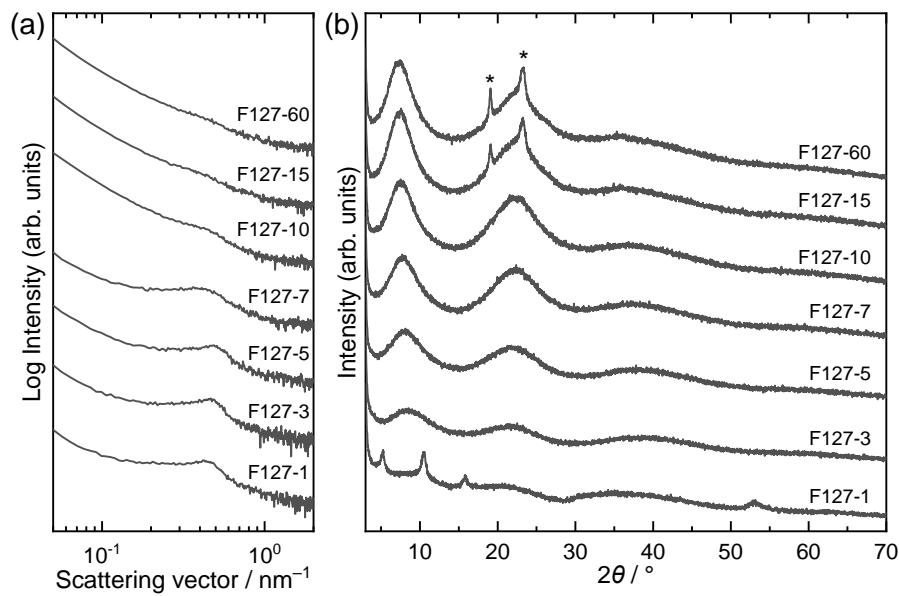
Figure 4. (a) SAXS and (b) XRD patterns of dried powders of F127-1, F127-3, F127-5, F127-7, F127-10, F127-15, and F127-60. *: peaks assigned to the crystalline polyethylene oxide chain of F127.[34]
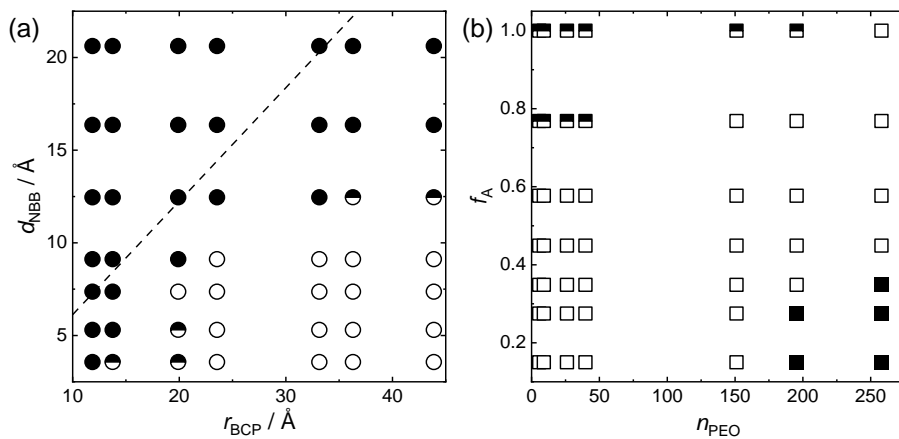
Figure 5. Summary of (a) meso-periodicity and (b) formed crystals of prepared powders; relationship between (a) r_{BCP} and d_{NBB} and (b) n_{PEO} and f_A. Symbols in (a); powders showed clear/broad/no SAXS peaks (open/half-filled/closed circle), and (b) powders composed of layered nickel hydroxides (open square), layered nickel hydroxides with BCP-based co-crystal (half-filled square), and layered nickel hydroxides with crystalline BCPs (closed square). Dashed line in (a) is critical d_{NBB} predicted in previous report[20].

13

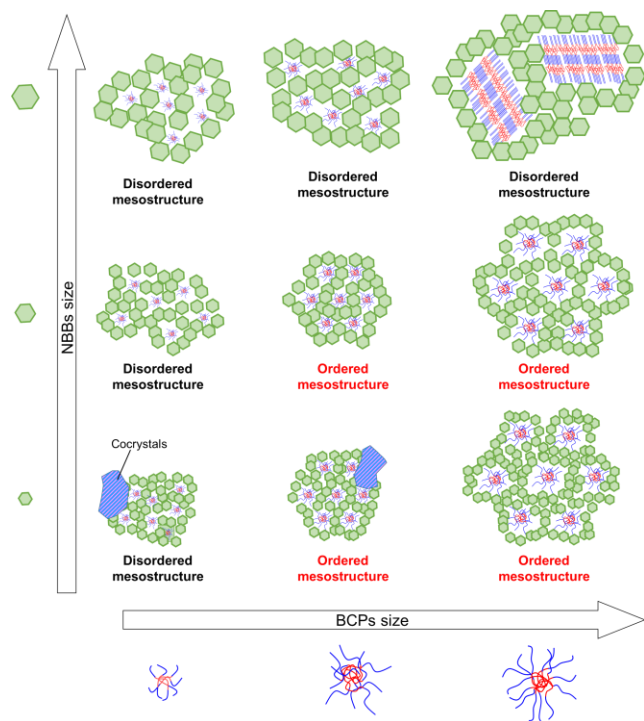**Figure 6.** Schematic illustration for the formation of ordered/disordered mesostructures using different sized hydroxide NBBs and templating BCPs.

Table 1. Characteristics of solution and formed NBBs during epoxide-mediated alkalinization.

t_R [a] / min	pH	σ [b] / mS cm^{-1}	d_{NBB} [c] / Å	f_A [d]	D_{NBB} [e] / Å
1	2.48	1.43	3.56	1.0	8.9
3	3.07	1.38	5.30	0.77	11.2
5	3.47	1.23	7.36	0.58	15.0
7	3.90	1.02	9.12	0.45	17.2
10	4.61	0.717	12.5	0.35	18.9
15	5.46	0.359	16.4	0.28	20.6
60	6.41	0.104	20.6	0.15	19.7

[a] Reaction time, [b] conductivity of reacting solution; [c] diameter of NBBs; [d] relative amount of acrylic acid deduced from infrared absorbance bands of COO of acrylate and C=C of acrylic

acid; [e] crystallite size of NBBs. Diameter of NBBs and relative amount of acrylic acid were reported in other paper.[20] Copyright 2019 American Chemical Society.

Table 2. Characteristics of BCPs employed in the present study.

Pluronic BCPs	M_w [a] / g mol^{-1}	Molecular strcture [b]	M_{CMC} [c] / mol L^{-1}	r_{BCP} [d] / Å
F108	14600	$PEO_{129}PPO_{56}PEO_{129}$	2.2×10^{-5}	43.9
F127	12600	$PEO_{98}PPO_{69}PEO_{98}$	2.8×10^{-6}	36.3
F68	8400	$PEO_{76}PPO_{30}PEO_{76}$	4.8×10^{-4}	33.2
P123	5750	$PEO_{20}PPO_{69}PEO_{20}$	4.4×10^{-6}	23.6
L121	4400	$PEO_5PPO_{69}PEO_5$	1.0×10^{-6}	19.9
L64	2900	$PEO_{13}PPO_{30}PEO_{13}$	4.8×10^{-4}	13.8
L61	2000	$PEO_3PPO_{30}PEO_3$	1.1×10^{-4}	11.9

[a] Molecular weight provided by the manufacture (BASF Corp.); [b] PEO and PPO means polyethylene oxide blocks and polypropylene oxide blocks, respectively; [c] critical micelle concentration[39,41] Copyright 2000 American Chemical Society. Copyright 1995 with permission from Elsevier.; [d] gyration radius of BCPs dissolved in ethanolic solution (5 mmol/L)

ASSOCIATED CONTENT

Supporting Information. Characterization details of SAXS measurement, SAXS patterns, calculated gyration radius, SEM images, and XRD patterns of the prepared mesostructured and/or mesoporous materials.

AUTHOR INFORMATION

Corresponding Author

* E-mail: n-tarutani@hiroshima-u.ac.jp

Author Contributions

The manuscript was written through contributions of all authors. All authors have given approval to the final version of the manuscript. ‡These authors contributed equally. (match statement to author names with a symbol)

Notes

The authors declare no competing financial interest.

REFERENCES

(1)   Yanagisawa, T.; Shimizu, T.; Kuroda, K.; Kato, C. The Preparation of Alkyltriinethylaininonium–Kaneinite Complexes and Their Conversion to Microporous Materials. *Bull. Chem. Soc. Jpn.* **1990**, *63*, 988–992.

(2)   Soler-Illia, G. J. A. A.; Innocenzi, P. Mesoporous Hybrid Thin Films: The Physics and Chemistry Beneath. *Chem. - A Eur. J.* **2006**, *12*, 4478–4494.

(3)   Li, W.; Liu, J.; Zhao, D. Mesoporous Materials for Energy Conversion and Storage Devices. *Nat. Rev. Mater.* **2016**, *1*, 16023.

(4)   de A. A. Soler-Illia, G. J.; Scolan, E.; Louis, A.; Albouy, P.-A.; Sanchez, C. Design of Meso-Structured Titanium Oxo Based Hybrid Organic–Inorganic Networks. *New J. Chem.* **2001**, *25*, 156–165.

(5)   Hwang, Y. K.; Kwon, Y.-U.; Lee, K.-C. Nanoparticle Routes to Mesoporous Titania Thin Films. *Chem. Commun.* **2001**, No. 18, 1738–1739.

(6)   Wong, M. S.; Jeng, E. S.; Ying, J. Y. Supramolecular Templating of Thermally Stable Crystalline Mesoporous Metal Oxides Using Nanoparticulate Precursors. *Nano Lett.* **2001**, *1*, 637–642.

(7)   Carretero-Genevrier, A.; Gich, M.; Picas, L.; Gazquez, J.; Drisko, G. L.; Boissiere, C.; Grosso, D.; Rodriguez-Carvajal, J.; Sanchez, C. Soft-Chemistry-Based Routes to Epitaxial a-Quartz Thin Films with Tunable Textures. *Science* **2013**, *340*, 827–831.

(8)   Armatas, G. S.; Kanatzidis, M. G. Hexagonal Mesoporous Germanium. *Science* **2006**, *313*, 817–820.

(9)   Warren, S. C.; Messina, L. C.; Slaughter, L. S.; Kamperman, M.; Zhou, Q.; Gruner, S. M.; DiSalvo, F. J.; Wiesner, U. Ordered Mesoporous Materials from Metal Nanoparticle-Block Copolymer Self-Assembly. *Science* **2008**, *320*, 1748–1752.

(10)   Chane-Ching, J. Y.; Cobo, F.; Aubert, D.; Harvey, H. G.; Airiau, M.; Corma, A. A General Method for the Synthesis of Nanostructured Large-Surface-Area Materials through the Self-Assembly of Functionalized Nanoparticles. *Chem. - A Eur. J.* **2005**, *11*, 979–987.

(11)   Tarutani, N.; Tokudome, Y.; Jobbágy, M.; Viva, F. A.; Soler-Illia, G. J. A. A.; Takahashi, M. Single-Nanometer-Sized Low-Valence Metal Hydroxide Crystals: Synthesis via

Epoxide-Mediated Alkalinization and Assembly toward Functional Mesoporous Materials. *Chem. Mater.* **2016**, *28*, 5606–5610.

(12)   Oka, Y.; Kuroda, Y.; Matsuno, T.; Kamata, K.; Wada, H.; Shimojima, A.; Kuroda, K. Preparation of Mesoporous Basic Oxides through Assembly of Monodispersed Mg–Al Layered Double Hydroxide Nanoparticles. *Chem. - A Eur. J.* **2017**, *23*, 9362–9368.

(13)   Jiang, Y.-F.; Jiang, N.; Liang, K.; Yuan, C.-Z.; Fang, X.-X.; Xu, A.-W. A Simple and General Route to Prepare Functional Mesoporous Double-Metal Oxy(Hydroxide). *J. Mater. Chem. A* **2019**, *7*, 7932–7938.

(14)   Yuranov, I.; Moeckli, P.; Suvorova, E.; Buffat, P.; Kiwi-minsker, L.; Renken, A. Pd/SiO 2 Catalysts: Synthesis of Pd Nanoparticles with the Controlled Size in Mesoporous Silicas. *J. Mol. Catal. A Chem.* **2003**, *192*, 239–251.

(15)   Wu, Y.; Cheng, G.; Katsov, K.; Sides, S. W.; Wang, J.; Tang, J.; Fredrickson, G. H.; Moskovits, M.; Stucky, G. D. Composite Mesostructures by Nano-Confinement. *Nat. Mater.* **2004**, *3*, 816–822.

(16)   Solveyra, E. G.; De La Llave, E.; Molinero, V.; Soler-Illia, G. J. A. A.; Scherlis, D. A. Structure, Dynamics, and Phase Behavior of Water in TiO2 Nanopores. *J. Phys. Chem. C* **2013**, *117*, 3330–3342.

(17)   Velasco, M. I.; Franzoni, M. B.; Franceschini, E. A.; Gonzalez Solveyra, E.; Scherlis, D.; Acosta, R. H.; Soler-Illia, G. J. A. A. Water Confined in Mesoporous TiO2 Aerosols: Insights from NMR Experiments and Molecular Dynamics Simulations. *J. Phys. Chem. C* **2017**, *121*, 7533–7541.

(18)   Murai, S.; Uno, S.; Kamakura, R.; Ishii, S.; Nagao, T.; Fujita, K.; Tanaka, K. Plasmonic Mesostructures with Aligned Hotspots on Highly Oriented Mesoporous Silica Films. *Opt. Mater. Express* **2016**, *6*, 2824.

(19)   Wang, Y. W.; Kao, K. C.; Wang, J. K.; Mou, C. Y. Large-Scale Uniform Two-Dimensional Hexagonal Arrays of Gold Nanoparticles Templated from Mesoporous Silica Film for Surface-Enhanced Raman Spectroscopy. *J. Phys. Chem. C* **2016**, *120*, 24382–24388.

(20)   Tarutani, N.; Tokudome, Y.; Jobbágy, M.; Soler-Illia, G. J. A. A.; Tang, Q.; Müller, M.; Takahashi, M. Highly Ordered Mesoporous Hydroxide Thin Films through Self-Assembly of Size-Tailored Nanobuilding Blocks: A Theoretical-Experimental Approach. *Chem. Mater.* **2019**, *31*, 322–330.

(21)   Gash, A. E.; Tillotson, T. M.; Satcher, J. H.; Poco, J. F.; Hrubesh, L. W.; Simpson, R. L. Use of Epoxides in the Sol - Gel Synthesis of Porous Iron (III) Oxide Monoliths from Fe (III) Salts. *Chem. Mater.* **2001**, *13*, 999–1007.

(22)   Oestreicher, V.; Jobbágy, M. One Pot Synthesis of Mg 2 Al(OH) 6 Cl·1.5H 2 O Layered Double Hydroxides: The Epoxide Route. *Langmuir* **2013**, *29*, 12104–12109.

(23)   Oestreicher, V.; Fábregas, I.; Jobbágy, M. One-Pot Epoxide-Driven Synthesis of M2Al(OH)6Cl·1.5H2O Layered Double Hydroxides: Precipitation Mechanism and Relative Stabilities. *J. Phys. Chem. C* **2014**, *118*, 30274–30281.

(24)   Oestreicher, V.; Hunt, D.; Torres-Cavanillas, R.; Abellán, G.; Scherlis, D. A.; Jobbágy, M. Halide-Mediated Modification of Magnetism and Electronic Structure of α-Co(II) Hydroxides: Synthesis, Characterization, and DFT+U Simulations. *Inorg. Chem.* **2019**, *58*, 9414–9424.

(25)   Beaucage, G.; Schaefer, D. W. Structural Studies of Complex Systems Using Small-Angle Scattering: A Unified Guinier/Power-Law Approach. *J. Non. Cryst. Solids* **1994**, *172–174*, 797–805.

(26)   Beaucage, G. Approximations Leading to a Unified Exponential/Power-Law Approach to Small-Angle Scattering. *J. Appl. Crystallogr.* **1995**, *28*, 717–728.

(27)   Nawaz, S.; Carbone, P. Coarse-Graining Poly(Ethylene Oxide)–Poly(Propylene Oxide)–Poly(Ethylene Oxide) (PEO–PPO–PEO) Block Copolymers Using the MARTINI Force Field. *J. Phys. Chem. B* **2014**, *118*, 1648–1659.

(28)   Hvidt, S.; Jørgensen, E. B.; Brown, W.; Schulen, K. Micellization and Gelation of Aqueous Solutions of a Triblock Copolymer Studied by Rheological Techniques and Scanning Calorimetry. *J. Phys. Chem.* **1994**, *98*, 12320–12328.

(29)   Glatter, O.; Scherf, G.; Schillén, K.; Brown, W. Characterization of a Poly(Ethylene Oxide)-Poly(Propylene Oxide) Triblock Copolymer (EO27-PO39-EO27) in Aqueous Solution. *Macromolecules* **1994**, *27*, 6046–6054.

(30)   Soler-Illia, G. J. D. A. A.; Louis, A.; Sanchez, C. Synthesis and Characterization of Mesostructured Titania-Based Materials through Evaporation-Induced Self-Assembly. *Chem. Mater.* **2002**, *14*, 750–759.

(31)   Zhong, Z.; Guo, C.; Chen, L.; Xu, J.; Huang, Y. Co-Crystal Formation between Poly(Ethylene Glycol) and a Small Molecular Drug Griseofulvin. *Chem. Commun.* **2014**, *50*, 6375–6378.

(32)   Ploszajski, A. R.; Billing, M.; Cockcroft, J. K.; Skipper, N. T. Crystalline Structure of an Ammonia Borane–Polyethylene Oxide Cocrystal: A Material Investigated for Its Hydrogen Storage Potential. *CrystEngComm* **2018**, *20*, 4436–4440.

(33)   Chappa, P.; Maruthapillai, A.; Voguri, R.; Dey, A.; Ghosal, S.; Basha, M. A. Drug-
         Polymer Co-Crystals of Dapsone and Polyethylene Glycol: An Emerging Subset in
         Pharmaceutical Co-Crystals. *Cryst. Growth Des.* **2018**, *18*, 7590–7598.

(34)   Innocenzi, P.; Malfatti, L.; Marcelli, A.; Piccinini, M. Evaporation-Induced Crystallization
         of Pluronic F127 Studied in Situ by Time-Resolved Infrared Spectroscopy. *J. Phys. Chem.
         A* **2010**, *114*, 304–308.

(35)   Tarutani, N.; Tokudome, Y.; Nakanishi, K.; Takahashi, M. Layered Double Hydroxide
         Composite Monoliths with Three-Dimensional Hierarchical Channels: Structural Control
         and Adsorption Behavior. *RSC Adv.* **2014**, *4*, 16075–16080.

(36)   Tarutani, N.; Tokudome, Y.; Jobbágy, M.; Soler-Illia, G. J. A. A.; Takahashi, M.
         Mesoporous Microspheres of Nickel-Based Layered Hydroxides by Aerosol-Assisted
         Self-Assembly Using Crystalline Nano-Building Blocks. *J. Sol-Gel Sci. Technol.* **2019**, *89*,
         216–224.

(37)   Bornside, D. E.; Macosko, C. W.; Scriven, L. E. Spin Coating: One-dimensional Model. *J.
         Appl. Phys.* **1989**, *66*, 5185–5193.

(38)   Nandiyanto, A. B. D.; Okuyama, K. Progress in Developing Spray-Drying Methods for
         the Production of Controlled Morphology Particles: From the Nanometer to
         Submicrometer Size Ranges. *Adv. Powder Technol.* **2011**, *22*, 1–19.

(39)   Kozlov, M. Y.; Melik-Nubarov, N. S.; Batrakova, E. V.; Kabanov, A. V. Relationship
         between Pluronic Block Copolymer Structure, Critical Micellization Concentration and
         Partitioning Coefficients of Low Molecular Mass Solutes. *Macromolecules* **2000**, *33*,
         3305–3313.

(40)   García Daza, F. A.; Colville, A. J.; Mackie, A. D. Mean-Field Coarse-Grained Model for Poly(Ethylene Oxide)-Poly(Propylene Oxide)-Poly(Ethylene Oxide) Triblock Copolymer Systems. *Langmuir* **2015**, *31*, 3596–3604.

(41)   Alexandridis, P.; Alan Hatton, T. Poly(Ethylene Oxide)-Poly(Propylene Oxide)-Poly(Ethylene Oxide) Block Copolymer Surfactants in Aqueous Solutions and at Interfaces: Thermodynamics, Structure, Dynamics, and Modeling. *Colloids Surfaces A Physicochem. Eng. Asp.* **1995**, *96*, 1–46.

TOC Graphic

Large BCPs Small NBBs Small BCPs Large NBBs

Co-Assembly

Ordered mesostructure Disordered mesostructure